Effect of spatially oscillating field on Schwinger pair production

Orkash Amat,[1] Li-Na Hu,[1] Mamat Ali Bake,[2] Melike Mohamedsedik,[3] and B. S. Xie[1,4,*]

[1]*Key Laboratory of Beam Technology of the Ministry of Education and College of Nuclear Science and Technology, Beijing Normal University, Beijing 100875, China*
[2]*School of Physics Science and Technology, Xinjiang University, Urumqi 830046, China*
[3]*College of Xinjiang Uyghur Medicine, Hotan 848000, China*
[4]*Institute of Radiation Technology, Beijing Academy of Science and Technology, Beijing 100875, China*

(Received 15 May 2023; accepted 31 August 2023; published 15 September 2023)

Effect of spatially oscillating field on Schwinger pair production is studied numerically and analytically when the work done by the electric field over its spatial extent is smaller than twice the electron mass. Under large spatial scale, we explain the characteristics of the position and momentum distribution of created pairs via the tunneling picture for the Dirac vacuum. Moreover, the exact Dirac-Heisenberg-Wigner formalism can be simplified by some alternative methods such as local density approximation, analytical approximation, and locally constant field approximation when the spatial scale is large in a certain of spatial oscillating cycle number. Also, the validity of these alternative methods are illustrated and discussed. For the studied spatially oscillating field, our results show that the maximum reduced particle number is about 5 times in comparison with the maximum one of nonoscillating inhomogeneous field.

DOI: 10.1103/PhysRevD.108.056011

I. INTRODUCTION

Schwinger effect is one of the fascinating nonperturbative phenomena in quantum electrodynamics (QED) [1–5]. This effect has not been yet observed directly in the laboratory as the critical field strength $E_{\mathrm{cr}} = m^2c^3/e\hbar \approx 1.3 \times 10^{16}$ V/cm (corresponding laser intensity is about 4.3×10^{29} W/cm^2, where m and $-e$ are the electron mass and charge) is not feasible so far [6–8]. With the rapid development of laser technology, however, the forthcoming laser intensity [9,10] is expected to reach 10^{24}–10^{26} W/cm^2, which has raised hopes of observing pair production in the future [11].

The effects of spacetime-dependent inhomogeneous fields on pair production is an interesting issue for studies in the strong field QED. It is known that the different spatial or temporal shapes of the field have different effects on the pair production [12,13], e.g., temporal Sauter envelope [14], spatial Sauter envelope [15], temporal super-Gaussian envelope [16], spatial Gaussian envelope [17], etc. Additionally, the influence of different field parameters is also important, e.g., frequency chirp effect [18–20] and phase effect [21]. For the non-plane-wave background field, there are many studies for either some simple spatial inhomogeneous fields like the cosine, Sauter, and Gaussian shapes [15–20] or some time-dependent fields with temporal shapes [22–25].

As we mentioned earlier, the different temporal or spatial shapes of the field have different effects on the pair production. Though there are many studies on it, there are still a series of problems. For example, in Refs. [26–30], the effect of spatial or temporal oscillating field on pair production is investigated, while for the spatial oscillating field, the coupling effect of spatial scale and spatial oscillation on pair production needs further study. Among them there is a special case, in which the work done by the electric field over its spatial extent (we denote it W) may be smaller than twice the electron mass. In this special case, however, the previous studies [31–34] are focused mainly on the fields with Gaussian-like shapes. To our knowledge, an effect of the spatially oscillating inhomogeneous field on the pair production is still lacking enough research, therefore, it is necessary to study the effect of spatially oscillating field in the specific $W < 2mc^2$.

Under such circumstance, we intend to study and answer some of the involved problems. For example, what will happen to the distribution of pair production? Will the local density approximation (LDA) be applied to it? Can the LDA be explained by analytical approximation (AA)? What is the difference between LDA, AA, and locally constant field approximation (LCFA)? On the other hand, the tunneling picture has played a key role in the vacuum pair production beside the multiphoton mechanism for the temporal oscillating field when $\hbar\omega \le 2mc^2$, where ω is the

*bsxie@bnu.edu.cn

field frequency [31], which has been seen from the study of some interesting fields [35]. Thus, it would be also helpful to understand the results of present research from the viewpoint of tunneling time and distance.

It is necessary to give a simple introduction to some of the widely used and powerful tools that can calculate particle distribution in spatial oscillating inhomogeneous fields. Among many methods to investigate pair production, as far as we know, some important ones include the worldline instanton (WI) technique [36–51], real-time Dirac-Heisenberg-Wigner (DHW) formalism [52–56], computational quantum field theory [57–61], imaginary-time method [62], quantum Vlasov equation (QVE) [63–67], Wentzel-Kramers-Brillouin approach [68–71], scattering matrix approach [72–84], and so on. It is noticed that the DHW formalism allows us to investigate the pair production for any background field [16]. On the other hand, due to the nature of the pair production under a spacetime-dependent field, one can find only a few analytical results for simple background modes [35,85–88]. Hence, we have to adopt numerical methods to study various natures of pair production. In the present work, we will use the DHW formalism as our numerical approach.

Motivated by the factors mentioned above, in this paper, we investigate the vacuum pair production when $W < 2mc^2$. First, we give a simple perspective picture which reveals mainly the tunneling process. We further demonstrate its correctness for the pair production via different numerical approaches and analytical approximation. We interpret why and how the electron-positron pair can create from the vacuum. Moreover, we present and discuss the exact tunneling distance and time of the created particle, which is employed to understand the characteristics of the position and momentum distribution of created pairs. We further show a relationship between the position distribution and tunneling time by employing the WI approach. Finally, we study the validity of LDA, AA, and LCFA [89] by comparing with the exact DHW result for large spatial scale.

The paper is organized as follows. In Sec. II, we briefly introduce the background field and tunneling picture in the Dirac vacuum. In Sec. III, numerical and analytical approaches are introduced. In Sec. IV, we derive the analytical solution of the tunneling time for large spatial scale via the WI technique. In Sec. V, we give and discuss our numerical and analytical results and interpret the momentum and position distributions of created pairs. Meanwhile, we show the relationship between the tunneling time and position distribution and explain the position distribution. In Sec. VI, we compare the results of LDA, AA, and LCFA with those of DHW formalism at large spatial scale and discuss the validity of them. Finally, the summary is given in Sec. VII.

We use the natural units ($\hbar = c = 1$) throughout this paper and express all quantities in terms of the electron mass m.

II. BACKGROUND FIELD AND TUNNELING PICTURE IN THE DIRAC VACUUM

A. Background field

In order to better understand, we consider an example of a spacetime-dependent spatially oscillating electric field. In our study, we ignore particle momenta orthogonal to this dominant direction [32]. We choose the scalar potential gauge $A^\mu(x,t) = (A^0, \mathbf{A}) = (\phi(x)f(t), 0, 0, 0)$. The electric field can be written as

$$E(x,t) = -\nabla A^0 = \varepsilon E_{\rm cr} g(x) f(t), \tag{1}$$

where $g(x) = \cos(kx)\mathrm{e}^{-\frac{x^2}{2\lambda^2}}$ and $f(t) = \mathrm{sech}^2(t/\tau)$, τ is pulse duration, ε is the peak field strength, $E_{\rm cr}$ denotes the Schwinger critical field strength, λ is spatial scale, k is the spatial wave number, and $\sigma_\lambda = k\lambda$ is the spatial oscillating cycle number. Accordingly, the spatial part of the corresponding scalar potential is

$$\phi(x) = -\frac{\sqrt{\pi}\lambda}{\sqrt{8}} e^{-\frac{1}{2}k^2\lambda^2}\left(\mathrm{erf}\left(\frac{x - ik\lambda^2}{\sqrt{2}\lambda}\right) + \mathrm{erf}\left(\frac{x + ik\lambda^2}{\sqrt{2}\lambda}\right)\right). \tag{2}$$

To have better comparable optimization schemes, we consider the external field which has the same energy in the spacetime with different k, λ, and τ, so that we define a baseline $\varepsilon_0 = 0.5$ when $k = 0$. Then the energy area density of the external field would keep the same as

$$\mathcal{E} \sim \int\int E^2(x,t)dxdt = \text{constant}. \tag{3}$$

From it we can obtain the peak field strength for different k as

$$\varepsilon(k,\lambda) = \sqrt{\frac{2}{1 + e^{-k^2\lambda^2}}}\varepsilon_0. \tag{4}$$

In Fig. 1, symbols A and B represent $W \geq 2mc^2$ and $W < 2mc^2$ cases, respectively. Note that the vacuum pair production in the regime of A is well understood in many previous works [32–34], but the pair creation in regimes of B lacks enough study, which is the focusing parameters range in the present research.

B. Tunneling picture in the Dirac vacuum

The electron-positron pair will create from the vacuum after the particle jumps from any negative high energy state at $x_+ = x + \Delta x$ to any positive low energy state at $x_- = x - \Delta x$ in the Dirac semiclassical picture of the vacuum when the work $W = e\int \mathbf{E}\cdot d\mathbf{x} < 2mc^2$ as shown in Fig. 2. The electron position distribution depends on the center-of-mass coordinate x [52], thus, we will consider the above transition probability of the particle at x in order to interpret

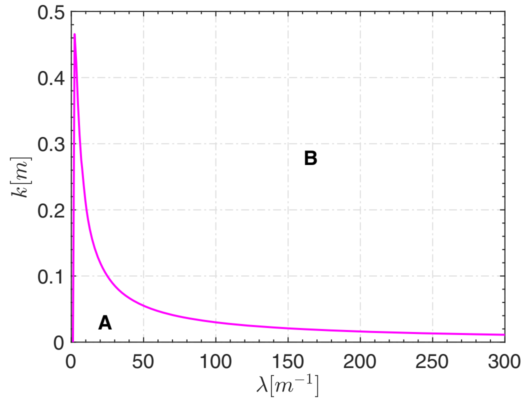

FIG. 1. Plot of the work W for k and λ. Areas A and B represent $W \geq 2mc^2$ and $W < 2mc^2$, respectively. The magenta line denotes $W = 2mc^2$.

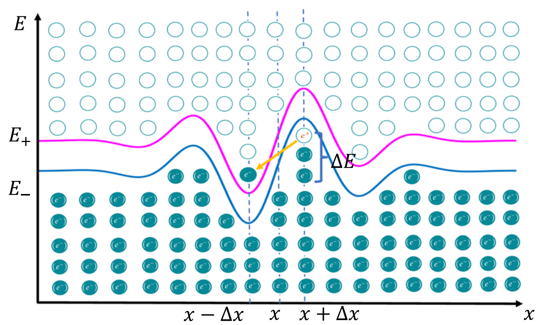

FIG. 2. Plot for the Dirac vacuum under high spatial oscillating spacetime-dependent electric field, where $E_\pm(x) = \pm mc^2 + \phi(x)$ when $W < 2mc^2$, where $\phi(x)$ is the spatial part of the scalar potential of the background field as shown in Eq. (2). The magenta and blue lines denote the $E_+(x)$ (minimum positive energy band) and $E_-(x)$ (maximum negative energy band) for the same center-of-mass coordinate x, respectively.

the position and momentum distributions of electron. Moreover, we can obtain the transition (tunneling) distance $d = x_+ - x_- = 2\Delta x$, see Fig. 2. Note that this quantum jumping process includes the tunneling process under an external spatial oscillating spacetime-dependent field. The energy gap between the two energy bands ΔE is transformed into the created pair's energy. From energy conservation of this process, $\Delta E = E_{e^-} + E_{e^+}$, we can find the general relativistic relation under the pure external field (does not include the ponderomotive force and charge density [32,34]) as

$$\left(\frac{\Delta E}{2}\right)^2 = m_*^2 + p^2, \tag{5}$$

where m_* is effective mass [90], and p represents the kinetic momenta [20]. According to our new perspective picture, the electron-positron pair can escape successfully from the vacuum by jumping from the negative high energy state to the positive low energy state when $W < 2mc^2$. This is why the electron-positron pairs can get out of the vacuum. In this work, we only consider the maximum transition probability (positive and negative energy gap is maximum) in order to interpret the maximum of the momentum distribution. The maximum energy gap is $\Delta E = E_-(x) - E_+(x)$ in Fig. 2, and these energy bands can be written as $E_\pm(x) = \pm mc^2 + \phi(x)$.

III. NUMERICAL AND ANALYTICAL METHODS

A. DHW formalism

For studying the electron-positron pair production of vacuum in the background fields, we write the Lagrangian [33]

$$L(\Psi,\bar{\Psi},A) = \frac{i}{2}(\bar{\Psi}\gamma^\mu\mathcal{D}_\mu\Psi - \bar{\Psi}\mathcal{D}_\mu^\dagger\gamma^\mu\Psi) - m\bar{\Psi}\Psi - \frac{1}{4}F_{\mu\nu}F^{\mu\nu}, \tag{6}$$

where $\mathcal{D}_\mu = (\partial_\mu + ieA_\mu)$ is the covariant derivative and correspondingly $\mathcal{D}_\mu^\dagger = (\overleftarrow{\partial_\mu} - ieA_\mu)$. In order to describe the dynamics of the particles, we need the Dirac equation

$$(i\gamma^\mu\partial_\mu - e\gamma^\mu A_\mu(r) - m)\Psi(r) = 0, \tag{7}$$

and the adjoint Dirac equation

$$\bar{\Psi}(r)(i\gamma^\mu\overleftarrow{\partial_\mu} + e\gamma^\mu A_\mu(r) + m) = 0. \tag{8}$$

The Dirac spinors Ψ, $\bar{\Psi}$ and the vector potential $A^\mu(r)$ are the main ingredients in the DHW formalism. Note that the background is considered to be a classical one. Further, we introduce the density operator as [33]

$$\hat{\mathcal{C}}_{\alpha\beta}(r,s) = \mathcal{U}(A,r,s)[\bar{\Psi}_\beta(r - s/2), \Psi_\alpha(r + s/2)], \tag{9}$$

where r and s denote the center-of-mass and the relative coordinate of two particles. The Wilson line factor is used to make the density operator gauge invariant under the $U(1)$ gauge [32]

$$\mathcal{U}(A,r,s) = \exp\left(ies\int_{-1/2}^{1/2} d\xi A(r + \xi s)\right). \tag{10}$$

In order to perform numerical calculations, we use the DHW formalism as the powerful tool in our study because it allows us to investigate vacuum pair production for the inhomogeneous field [52]. Note that only the equal-time Wigner function can be used to get the needed evolution of the system for the studied problem of pair production [48]; thus, all the quantities are for the components of the equal-time Wigner function in the following, even if they are still denoted as an uppercase letter. Now we can apply the DHW formalism to the case of one spatial dimension, in which there are only four Wigner components, $\mathbb{S}$, $\mathbb{V}_0$, $\mathbb{V}_x$, and $\mathbb{P}$ for electric field $E(x,t)$. The DHW equations of motion in this case of $1+1$ can be written as [32]

$$D_t\mathbb{S} - 2p_x\mathbb{P} = 0, \tag{11}$$

$$D_t\mathbb{V}_0 + \partial_x\mathbb{V}_x = 0, \tag{12}$$

$$D_t\mathbb{V}_x + \partial_x\mathbb{V}_0 = -2\mathbb{P}, \tag{13}$$

$$D_t\mathbb{P} + 2p_x\mathbb{S} = 2m\mathbb{V}_x, \tag{14}$$

where

$$D_t = \partial_t + e\int_{-1/2}^{1/2} d\xi E_x(x + i\xi\partial_{p_x}, t)\partial_{p_x}. \tag{15}$$

Here, $\mathbb{S}$ is mass density, $\mathbb{V}_0$ is charge density, $\mathbb{V}_x$ is current density, and $\mathbb{P}$ is somewhat associated to pseudoscalar condensation [33,34,54,91]. Note that the role of transverse momentum of particles is that it determines directly the current density on the transverse momentum direction. Theoretically, one could take into account the transverse momentum in the involved research, but we ignore it in our present study due to two main reasons. The first one is that the transverse momentum has little effect on the problem we are studying. Since the direction of the electric field is along the x axis and the particle appears mainly in the direction of the electric field, the study can thereby be simplified to the case where the transverse momentum is assumed to be zero [19,32,54]. The second one is that, if the transverse momentum is taken into account, the dimension of our DHW formula will be high, which will lead to a very large amount of computation work [16,26].

In order to perform simulation more conveniently, we can define four Wigner components as $\mathbb{W}_0 = \mathbb{S}$, $\mathbb{W}_1 = \mathbb{V}_0$, $\mathbb{W}_2 = \mathbb{V}_x = \mathbb{V}$, and $\mathbb{W}_3 = \mathbb{P}$. So from the initial conditions given by the vacuum solution for single particle,

$$\mathbb{S}^v(p_x) = -\frac{2}{\sqrt{1+p_x^2}}, \qquad \mathbb{V}^v(p_x) = -\frac{2p_x}{\sqrt{1+p_x^2}}, \tag{16}$$

where upper indicator "v" represents the vacuum initial condition [33] in our work. We have the modified Wigner components as

$$\mathbb{W}_i^v = \mathbb{W}_i - \mathbb{W}_i^v. \tag{17}$$

Finally, we can calculate the particle number density at asymptotic times $t_f \to +\infty$,

$$n(x, p_x, t\to+\infty) = \frac{\mathbb{S}^v + p_x\mathbb{V}_x^v}{\sqrt{1+p_x^2}}. \tag{18}$$

The momentum and position distributions are given by

$$n(p_x, t\to+\infty) = \int\frac{dx}{2\pi} n(x, p_x, t\to+\infty), \tag{19}$$

$$n(x, t\to+\infty) = \int dp_x n(x, p_x, t\to+\infty). \tag{20}$$

The total particle number is readily achieved by

$$N(t\to+\infty) = \int \mathrm{d}p_x n(p_x, t\to+\infty). \tag{21}$$

It is worth pointing out that for the convenient comparison we should cope with the reduced quantities $\bar{n}(p_x, t\to+\infty) = n(p_x, t\to+\infty)/\lambda$ and $\bar{N}(t\to+\infty) = N(t\to+\infty)/\lambda$ under the same energy.

B. LDA

When the spatial variation scale is much larger than the Compton wavelength $\lambda \gg \lambda_C$, the vacuum pair production can be described by LDA [32]. If the field is written as $E(x,t) = \varepsilon E_{\mathrm{cr}} g(x)h(t)$, then we can set $\varepsilon(x) = \varepsilon E_{\mathrm{cr}} g(x)$ as an effective field strength, where $h(t)$ is an arbitrary time-dependent function. We can obtain momentum and positron distributions by summing results for homogeneous fields with different field strengths given as [32]

$$\bar{n}_{\mathrm{loc}}(p_x, p_\perp, t\to+\infty) = \int\frac{dx}{2\pi}\bar{n}_{\mathrm{loc}}(\varepsilon(x)|p_x, p_\perp, t\to+\infty), \tag{22}$$

$$\bar{n}_{\mathrm{loc}}(x, t\to+\infty) = \int dp_x dp_\perp \bar{n}_{\mathrm{loc}}(\varepsilon(x)|p_x, p_\perp, t\to+\infty). \tag{23}$$

Note that $\bar{n}_{\mathrm{loc}}(\varepsilon(x)|p_x, p_\perp, t\to+\infty)$ in Eqs. (22) and (23) is a general form of the LDA in the multidimensional case. However, for our electric field, the dominant contribution on the Schwinger effect is along the direction of the electric field. Therefore, the transverse momentum $p_\perp$ is ignored, which reduces the multidimensional LDA form to the $1+1$-dimensional LDA one [32], i.e., $\bar{n}_{\mathrm{loc}}(\varepsilon(x)|p_x, 0, t\to+\infty) \coloneqq \bar{n}_{\mathrm{loc}}(\varepsilon(x)|p_x, t\to\infty)$. The $\bar{n}_{\mathrm{loc}}(\varepsilon(x)|p_x, t\to\infty)$ can be found by using quantum kinetic theory at any fixed point x for a time-dependent electric field $E(t) = \varepsilon(x)h(t)$ [32].

We choose the time-dependent spatial homogeneous DHW method to find one-particle distribution [92] and calculate the LDA result. The one-particle momentum distribution function $n(\mathbf{p}, t)$ can be obtained by solving the following ten ordinary differential equations and the nine auxiliary quantities $\mathbb{V}_i(\mathbf{p}, t)$, $\mathbb{A}_i(\mathbf{p}, t)$, and $\mathbb{T}_i(\mathbf{p}, t)$ [24,92]:

$$\begin{aligned}
\dot{n} &= \frac{e}{2\Omega}\mathbf{E}\cdot\mathsf{V},\\
\dot{\mathsf{V}} &= \frac{2}{\Omega^3}((e\mathbf{E}\cdot\mathbf{p})\mathbf{p} - e\Omega^2\mathbf{E})(n-1)\\
&\quad - \frac{(e\mathbf{E}\cdot\mathsf{V})\mathbf{p}}{\Omega^2} - 2\mathbf{p}\times\mathbb{A} - 2m\mathbb{T},\\
\dot{\mathbb{A}} &= -2\mathbf{p}\times\mathsf{V},\\
\dot{\mathbb{T}} &= \frac{2}{m}[m^2\mathsf{V} + (\mathbf{p}\cdot\mathsf{V})\mathbf{p}], \qquad (24)
\end{aligned}$$

where $\Omega = \sqrt{m^2+\mathbf{p}^2}$ is the total energy of the particle. $\mathbb{V}_i(\mathbf{p},t)$, $\mathbb{A}_i(\mathbf{p},t)$, and $\mathbb{T}_i(\mathbf{p},t)$ are the three-dimensional Wigner components, and $\mathsf{V}_i(\mathbf{p},t) = \mathbb{V}_i(\mathbf{p},t) - (1-n(\mathbf{p},t))\mathbb{V}_i^v(\mathbf{p},t)$, $i = 1,2,3$ represents the x, y, and z directions, respectively. We will drop the indices in $\mathbb{V}$, $\mathbb{A}$, $\mathbb{T}$, and V to improve readability. Note that V is related to three-dimensional current density $\mathbb{V}$ and one-particle distribution function n, thus, V is not current density, but the coupling function of the $\mathbb{V}$ and n. For our electric field, there is only the current density on the x direction; at that time, the current density on the x direction in Eq. (24) is the same as the current density in Eq. (12). Initial condition values are selected as $n(\mathbf{p},-\infty) = \mathsf{V}(\mathbf{p},-\infty) = \mathbb{A}(\mathbf{p},-\infty) = \mathbb{T}(\mathbf{p},-\infty) = 0$ in order to perform the calculation. We can further obtain the one-particle momentum distribution $n(\mathbf{p},t)$.

It is worthy to note that, in our simulation, the Runge-Kutta method of 8(5, 3) order is used in order to avoid unphysical results during numerical calculation, in which we used $\mathrm{RelTol} = \mathrm{AbsTol} = 10^{-10}$ (where we have specified a relative tolerance RelTol as well as an absolute error tolerance AbsTol). In order to calculate the various distributions with high accuracy, the lattice sizes have been set to $N_x\times N_{p_x} = 8192\times 4096$ and $N_x\times N_{p_x} = 16384\times 4096$ for low and high spatial oscillating fields. Meanwhile, we have considered the range of wave number k and spatial scale λ as $0\leq k\leq 0.1$ m and $1.6\leq\lambda\leq 300\,\mathrm{m}^{-1}$, respectively. The grid sizes have been set as $N_k\times N_\lambda = 20\times 50$ in the work.

C. Analytical approximation for large spatial scale

The result can be obtained analytically by replacing the field strength ε in the analytical one-particle distribution solution with an effective field strength $\varepsilon(x) = \varepsilon E_{\mathrm{cr}} g(x)$ in the spacetime-dependent field when the field spatial scale is large. For example, we can get the analytical solution explicitly for $E(x,t) = \varepsilon E_{\mathrm{cr}} g(x)\mathrm{sech}^2(t/\tau)$ by replacing ε in the QVE solution for $E(t) = \varepsilon\mathrm{sech}^2(t/\tau)$ [33] with $\varepsilon(x)$ as [refer to Eq. (99) of Ref. [87]]

$$n(x,p_x,p_\perp,t\to+\infty) = \frac{2\sinh\left(\frac{\pi\tau}{2}[2e\tau\varepsilon(x)+\tilde{Q}(x)-Q(x)]\right)\sinh\left(\frac{\pi\tau}{2}[2e\tau\varepsilon(x)-\tilde{Q}(x)+Q(x)]\right)}{\sinh(\pi\tau\tilde{Q}(x))\sinh(\pi\tau Q(x))}, \qquad (25)$$

where

$$\tilde{Q}(x) = \sqrt{m^2+p_\perp^2+(p_x+2e\tau\varepsilon(x))^2}, \qquad (26)$$

$$Q(x) = \sqrt{m^2+p_\perp^2+(p_x-2e\tau\varepsilon(x))^2}. \qquad (27)$$

In the following, we denote this treatment as the analytical approximation for the large spatial scale approach. Here the transverse momentum $p_\perp$ is ignored in the AA for the $1+1$ case.

IV. TUNNELING TIME FOR LARGE SPATIAL SCALE

To interpret explicitly the features of the position distribution, one needs to introduce tunneling time for the spacetime-dependent inhomogeneous field when the spatial variation scale is much larger than the Compton wavelength $\lambda\gg\lambda_C$ (slowly varying envelope approximation). Note that our tunneling picture cannot directly calculate the tunneling time, but we can obtain it by using the WI technique in continuous position space and add to the shortcoming of the tunneling picture. The relationship between tunneling time in the Minkowski space and Euclidean space has been investigated in Ref. [35]. T_t is the tunneling time for any spacetime-dependent inhomogeneous fields, $x_\pm$ are the classical turning points, $x_4^{\min}$ and $x_4^{\max}$ are the maximum and minimum of the fourth WI path x_4 in the Euclidean space, and $\phi(x)$ is the potential of the field. From Ref. [35], we can know the definition of the tunneling time; the time taken by the particle from x_- to x_+ in the barrier region is tunneling time (quantum tunneling time). Further, we can achieve the tunneling time easily by performing Wick rotation in order to simplify the path integral via $x_4 = it$, see Ref. [15]. The tunneling time can be written as [35]

$$T_t = 2(x_4^{\max} - x_4^{\min}). \qquad (28)$$

If we choose the single-pulse time-dependent electric background,

$$E(t) = E\mathrm{sech}^2(t/\tau). \qquad (29)$$

The WI paths can be obtained in the scalar or spinor QED [15],

$$x_3(u) = \frac{m}{eE}\frac{1}{\gamma\sqrt{1+\gamma^2}}\operatorname{arcsinh}[\gamma\cos(2\pi u)], \tag{30}$$

$$x_4(u) = \frac{m}{eE}\frac{1}{\gamma}\arcsin\left[\frac{\gamma}{\sqrt{1+\gamma^2}}\sin(2\pi u)\right], \tag{31}$$

where $0 \le u \le 1$. Due to a lack of analytical solution, it is hard to obtain the analytical solution of the tunneling time directly under the spacetime-dependent inhomogeneous field. When the spatial variation scale is much larger than the Compton wavelength $\lambda \gg \lambda_C$, we can use spatial slowly varying envelope approximation. Thus, the tunneling time for the spacetime-dependent field can be locally described by replacing the ε in the analytical tunneling time solution under the time-dependent field with $\varepsilon(x) = \varepsilon E_{\rm cr} g(x)$. The tunneling time for our field could be obtained as

$$T_t(x) = 2\tau\arcsin\left[\frac{\gamma(x)}{\sqrt{1+\gamma^2(x)}}\right], \tag{32}$$

where

$$\gamma(x) = \frac{m}{e\tau|\varepsilon(x)|}. \tag{33}$$

Note that the tunneling time was obtained by using the WI technique [15], and obviously it is based on the Bohm viewpoint [93].

V. RESULTS

Now, we begin to prove the correctness of our perspective picture by adopting numerical and analytical methods. Here we use the DHW formalism and LDA and AA approaches.

The reduced total particle number achieved by the DHW, LDA, and AA approaches is shown in Fig. 3(a). Our results show that the maximum reduced particle number is about 5 times by comparing to that of [32], meanwhile, the maximum number corresponds to the parameter regime that belongs to area A. Interestingly, however, the particle number when $W < 2mc^2$ is still larger than the normal case ($k = 0$) in Fig. 3(a). On the other hand, the particle number when $k \neq 0$ is always larger than that when $k = 0$, by the way, in whole area A, we would recover the result to the Fig. 2 of Ref. [32]. Although the particle number is the same number for the same k and large space scale, we can find that the particle number for large λ decreases with the increase of k. This may be influenced by the spatial oscillating effect of the field on the pair production. Furthermore, the total particle distributions and maxima obtained from the three different approaches are

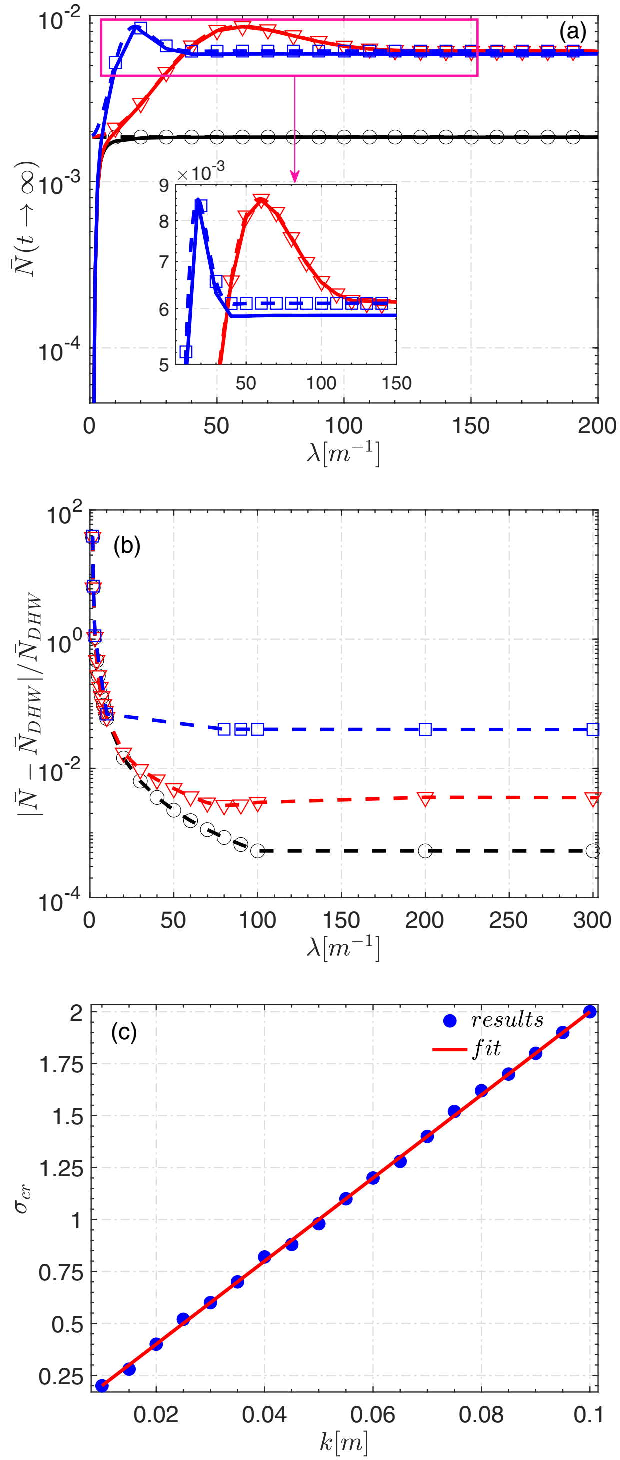

FIG. 3. Reduced total particle number (a) and error tolerance (b) with λ for different k. The solid line, dashed line, and symbols denote the DHW, LDA and AA results, respectively. The black line/circle, red line/triangle, and blue line/square correspond to $k = 0.00$, 0.03, and 0.10 m, respectively. $\bar{N}$ in (b) represents the LDA/AA result. (c) is the $\sigma_{\rm cr}$ with k, where the red line is a linear fit of the form $\sigma_{\rm cr}(k) \approx 20(k/m)$. Other parameters are $\varepsilon_0 = 0.5$ and $\tau = 10\,{\rm m}^{-1}$. Note that the field is chosen under the same field energy.

approximately the same for appropriate λ. From Fig. 3(b), we find that the error tolerance $|\bar{N} - \bar{N}_{\mathrm{DHW}}|/\bar{N}_{\mathrm{DHW}}$ is lower 3.8%, the reduced particle numbers obtained by the LAD and AA are the same as the DHW result when $\lambda \geq 20\,\mathrm{m}^{-1}$, where $\lambda_{\mathrm{cr}} = 20\,\mathrm{m}^{-1}$. We can further obtain a relationship between the critical spatial oscillating cycle number σ_{cr} and k, as shown in Fig. 3(c). We find that this relationship is linear and it can be fitted as $\sigma_{\mathrm{cr}}(k) \approx 20(k/m)$. When k is maximum ($k_{\max} = 0.1m$), $\sigma_{\mathrm{cr}}^{\max} = \sigma_{\mathrm{cr}}(k_{\max}) = 2$. For the whole situation, when $\sigma_{\mathrm{cr}} \geq 2$, the DHW, LDA, and AA results are the same.

Although the approximate same reduced total particle number is obtained by the different three methods of DHW formalism, LDA, and AA, it does not mean that the created pair experiences the same physical process. To see their differences, the momentum distribution is plotted in Fig. 4(a). While different approaches have different momentum distributions, they have almost the same area, which leads to the same total particle numbers approximately. Now we can interpret it by using our perspective picture mentioned in Sec. II, for example, the momentum corresponding to the maximum of the momentum distribution. As shown in Fig. 4(b), one notes that the electron in the negative energy state jumps from point A to point B, and during this process, the energy gap ΔE between A and B points would transform the energy to the created pair. At the same time, the transition probability of the electron is the largest because the transition probability is proportional to the energy gap ΔE and inversely proportional to the transition, i.e., tunneling, distance $d = x_B - x_A = 2\Delta x = \pi/k$, where x_B and x_A are the positions of A and B points in Fig. 4(b). Thus, the maximal energy gap could be found as $\Delta E = E_B - E_A \approx 12.1014$ m, where E_B and E_A denotes the energy for A and B points in Fig. 4(b), respectively. Then we can obtain $p \approx \pm 5.96749$ m appropriately for $x = 0$ point by using Eq. (5). Surprisingly, this value is just appropriately the momentum corresponding to the maximum of the momentum distribution for LDA formalism, i.e., $p_{\mathrm{peak}} \approx \pm 5.97215$ m in Fig. 4(a). We stress that, although the momentum distributions of the LDA and AA methods are exactly the same shape, the LDA and AA methods do not include the charge density as comparable to the DHW formalism where the charge density is present. The reason why the DHW result differs from those of LDA and AA is that the DHW formalism contains charge density $\mathbb{V}_0$, see Eq. (12), but the LDA and AA do not contain it, see Eq. (24).

It is emphasized that this does not mean that the tunneling picture is not really accurate together with LDA and AA in this case. From the reduced particle number in Fig. 3(a), we can see that the results obtained by the three methods of DHW, LDA, and AA are consistent with each other. In particular, the reduced particle number

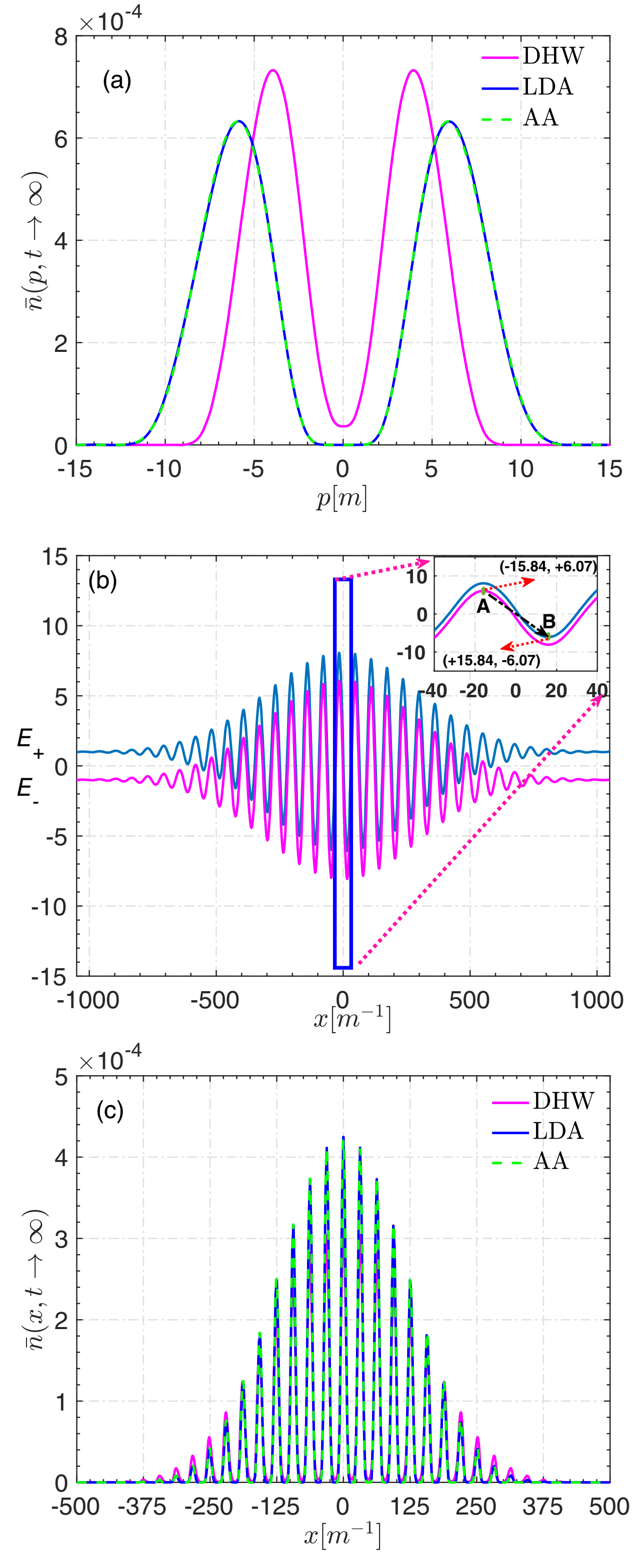

FIG. 4. Plots of momentum distribution (a), Dirac vacuum (b), and position distribution (c) when $W < 2mc^2$. The magenta, blue, and green dashed lines represent the DHW, LDA, and AA approaches, respectively, when $k = 0.1$ m, $\lambda = 300\,\mathrm{m}^{-1}$, and $\tau = 10\,\mathrm{m}^{-1}$.

in Fig. 3(a) is obtained from the particle number density by integrating over the whole phase space (the position and momentum space), see Eq. (21). From the above results, we can know that the tunneling picture is accurate together with LDA and AA. In this work, there are some difficulties in extending it to the more general considerations and more universal criteria. The reason is that, at small spatial scales, there is a strong influence of the ponderomotive force, which will lead to more complex physical processes in the tunneling picture. Therefore, in this paper, we only discuss the tunneling picture at large spatial scales.

Another interesting feature is that the particle position distribution, shown in Fig. 4(c), could be also understood via our perspective picture. From it one can find that strong oscillation occurs in the position distributions. To see the oscillatory phenomenon more clearly, we come back to Fig. 4(b) again and have an intuitive look at the maxima and minima transition probability at the center-of-mass coordinate x via our perspective picture. The essential point of these oscillations is the connection between the distance for transition probability from the maxima to minima around $x = M\pi/k$, where $M = 0, \pm1, \pm2, \pm3, \ldots$, which corresponds to jumping from peak to trough in Fig. 4(b), and the tunneling distance $d = 2\Delta x = \pi/k$. Obviously these two distances are the same. Similarly, around $x = (1/2 + M)\pi/k$, which corresponds to jumping from trough to peak in Fig. 4(b), the jump transition has the same tunneling distance $d = 2\Delta x = \pi/k$. This is why the oscillating effect appears in the position distributions. Of course, the results are completely the same with the results achieved by adopting $\bar{n}(x, t) \propto |\varepsilon E_{\rm cr} g(x) f(t)|^2$ according to Refs. [94,95]. This illustrates again that our perspective picture and its interpretation are reliable. Particularly note that it can not only offer the exact location (position) of the created particle, but also explain the characteristics of the position distribution.

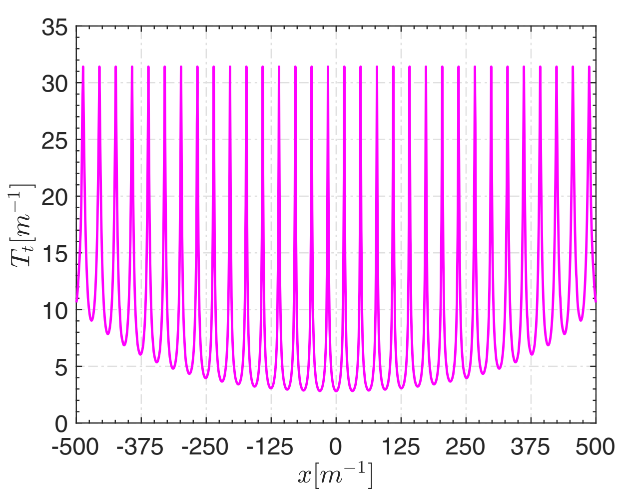

FIG. 5. Tunneling time for $k = 0.1$ m, $\lambda = 300$ m^{-1} and $\tau = 10$ m^{-1}.

Now let us to see why the classical tunneling picture is consistent with LDA and AA for the large spatial scales. There are two reasons for this. The first one is that the spatial Keldysh parameter is defined as $\gamma_k = mk/e\varepsilon(k,\lambda) = mk\sqrt{1+e^{-k^2\lambda^2}}/(\sqrt{2}e\varepsilon_0)$ [15]. When k is fixed, γ_k decreases with the increase of λ. It means that the tunneling process is more pronounced [15]. The second one is that the ponderomotive force is inversely proportional to the spatial scale [33]. When the spatial scale is very large, the ponderomotive force can be ignored. Because the LDA and AA just correspond to the case of large spatial scales, therefore, the force can be almost ignored. At the same time, our tunneling picture does not contain the ponderomotive force. This is why the classical tunneling picture is consistent with LDA and AA.

We can also interpret the oscillating effect in Fig. 4(c) by using tunneling time. An example of the tunneling time is shown in Fig. 5; we can observe that an obvious oscillating effect of the tunneling time and its minima and maxima corresponds to $x = M\pi/k$ and $x = (1/2 + M)\pi/k$, respectively, with an interval of $d = 2\Delta x = \pi/k$. Since the particle number is inversely proportional the tunneling time [35], we can find the self-consistent oscillating effect in the position distribution in Fig. 4(c). This can be regarded as another physical interpretation of the particle transition probability for every center-of-mass coordinate x. It should be pointed out that our new perspective picture provides us tunneling distance and the corresponding the tunneling time. On the contrary, the position of the created pair can be determined theoretically by the tunneling time. For instance, the position x in Fig. 5 corresponds to the position x in the position distribution plotting of Fig. 4(c).

The advantage of the tunneling time is that it can quickly estimate the properties of the particle position distribution, because the tunneling time includes all transition probabilities. In the next section, we will discuss the validity of the LDA, AA, and LCFA via the tunneling time.

VI. COMPARISON OF THE DHW FORMALISM, LDA, AA, AND LCFA

In this section, we discuss the validity of the LDA, AA, and LCFA [26] by comparing with the exact DHW result for large spatial scale. For short pulse duration $\tau = 5\,\mathrm{m}^{-1}$, the DHW formalism, LDA, and AA are the same distribution, but LCFA has different shape as shown in Fig. 6(a). However, for large pulse duration $\tau = 100\,\mathrm{m}^{-1}$, the DHW formalism, LDA, AA, and LCFA are the same shape as shown in Fig. 6(b). We further find that the positions corresponding to the minima of the tunneling time in Figs. 6(c) and 6(d) are consistent with the positions corresponding to the maxima of the position distribution

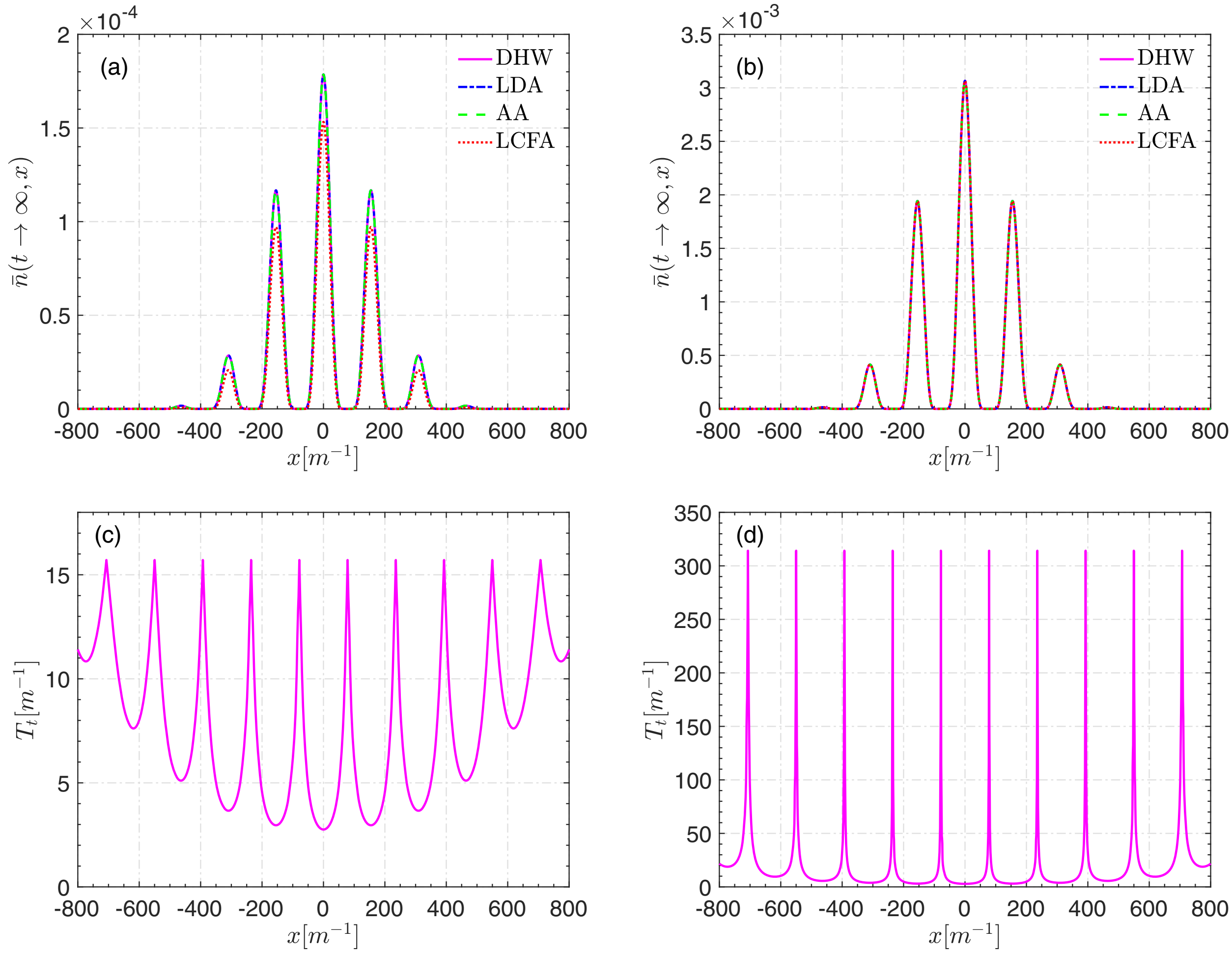

FIG. 6. Position distributions (first row) and tunneling time (second row). For each column, from left to right, $\tau = 5$ and $\tau = 100\ \mathrm{m}^{-1}$. Note the DHW formalism (magenta solid line), LDA (blue dash-dotted line), AA (green dashed line), and LCFA (red dotted) in (a) and (b). Other field parameters are $\varepsilon_0 = 0.5$, $\lambda = 400\ \mathrm{m}^{-1}$, and $k = 0.02$ m.

obtained by DHW formalism, LDA, AA, and LCFA in Figs. 6(a) and 6(b) because the particle number is inversely proportional to the tunneling time [35]. By the same way, the continuous variation of the position distribution could be also interpreted by using tunneling time, since the monotonicity of the position distribution is opposite to the monotonicity of the tunneling time.

VII. SUMMARY

In this work, we have studied numerically and analytically the effect of spatially oscillating field on Schwinger pair production when the work done by the electric field over its spatial extent is smaller than twice the electron mass. We have also given a representative example of the spacetime-dependent spatially oscillating electric field and introduced the tunneling picture. Moreover, we have investigated the validity of the LDA, AA, and LCFA. Our results are summarized briefly as follows.

First, we found that the total reduced particle number for the spatial oscillating inhomogeneous field is always larger than that for the nonspatial inhomogeneous oscillating field. Also, the maximum reduced particle number is about 5 times larger in comparison with the maximum one of the nonspatial oscillating inhomogeneous field. We further found that, when the spatial oscillating cycle number is larger than 2, the DHW, LDA, and AA results are the same for the whole situation. The momentum and position distributions have been interpreted by using a tunneling picture. Moreover, we show the relationship between the position distribution and tunneling time by employing the WI approach and explain the position distribution.

Second, we found that the LDA and AA hold when the spatial scale of the field is much larger than the electron Compton wavelength, while there is no restriction on the temporal scale of the field. However, the LCFA can be used when both spatial and temporal scales are much larger than the electron Compton wavelength λ_C and time t_C. This indicates that the LCFA has limitations on both spatial and temporal scales of the field. Therefore, LDA and AA are broader than LCFA. Finally, the properties of the particle position distribution have been estimated by the tunneling time.

ACKNOWLEDGMENTS

Some helpful discussions with A. Ilderton and C. Kohlfürst are acknowledged. We are also grateful to the anonymous referee for critical reading and helpful suggestions to improve the manuscript. This work was supported by the National Natural Science Foundation of China (NSFC) under Grants No. 12375240, No. 12265024, and No. 11935008. The computation was carried out at the HSCC of the Beijing Normal University.

[1] P. A. M. Dirac, The quantum theory of the electron, Proc. R. Soc. A **117**, 612 (1928).

[2] O. Klein, Die Reflexion von Elektronen an einem Potentialsprung nach der relativistischen Dynamik von Dirac, Z. Phys. **53**, 157 (1929).

[3] F. Sauter, Uber das Verhalten eines Elektrons im homogenen elektrischen Feld nach der relativistischen Theorie Diracs, Z. Phys. **69**, 742 (1931).

[4] W. Heisenberg and H. Euler, Consequences of Dirac's theory of positrons, Z. Phys. **98**, 714 (1936).

[5] J. S. Schwinger, On gauge invariance and vacuum polarization, Phys. Rev. **82**, 664 (1951).

[6] R. Alkofer, M. B. Hecht, C. D. Roberts, S. M. Schmidt, and D. V. Vinnik, Pair Creation and an X-Ray Free Electron Laser, Phys. Rev. Lett. **87**, 193902 (2001).

[7] F. Hebenstreit, R. Alkofer, G. V. Dunne, and H. Gies, Momentum Signatures for Schwinger Pair Production in Short Laser Pulses with Subcycle Structure, Phys. Rev. Lett. **102**, 150404 (2009).

[8] A. Ringwald, Pair production from vacuum at the focus of an x-ray free electron laser, Phys. Lett. B **510**, 107 (2001).

[9] Extreme light infrastructure (ELI), http://www.eli-beams.eu/.

[10] Exawatt center for extreme light studies (XCELS), http://xcels.iapras.ru.

[11] H. Abramowicz, U. Acosta, M. Altarelli, R. Aßmann, Z. Bai, T. Behnke, Y. Benhammou, T. Blackburn, S. Boogert, O. Borysov *et al.*, Conceptual design report for the LUXE experiment, Eur. Phys. J. Spec. Top. **230**, 2445 (2021).

[12] M. F. Linder, C. Schneider, J. Sicking, N. Szpak, and R. Schützhold, Pulse shape dependence in the dynamically assisted Sauter-Schwinger effect, Phys. Rev. D **92**, 085009 (2015).

[13] I. A. Aleksandrov, G. Plunien, and V. M. Shabaev, Pulse shape effects on the electron-positron pair production in strong laser fields, Phys. Rev. D **95**, 056013 (2017).

[14] V. S. Popov, Schwinger mechanism of electron positron pair production by the field of optical and x-ray lasers in vacuum, JETP Lett. **74**, 133 (2001).

[15] G. V. Dunne and C. Schubert, Worldline instantons and pair production in inhomogeneous fields, Phys. Rev. D **72**, 105004 (2005).

[16] C. Kohlfürst, Effect of time-dependent inhomogeneous magnetic fields on the particle momentum spectrum in electron-positron pair production, Phys. Rev. D **101**, 096003 (2020).

[17] M. Ababekri, B. S. Xie, and J. Zhang, Effects of finite spatial extent on Schwinger pair production, Phys. Rev. D **100**, 016003 (2019).

[18] L. J. Li, M. Mohamedsedik, and B. S. Xie, Enhanced dynamically assisted pair production in spatial inhomogeneous electric fields with the frequency chirping, Phys. Rev. D **104**, 036015 (2021).

[19] M. Mohamedsedik, L. J. Li, and B. S. Xie, Schwinger pair production in inhomogeneous electric fields with symmetrical frequency chirp, Phys. Rev. D **104**, 016009 (2021).

[20] L. N. Hu, O. Amat, L. J. Li, M. Mohamedsedik, and B. S. Xie, Pair production in inhomogeneous electric fields with phase modulation, Commun. Theor. Phys. **75**, 025102 (2023).

[21] M. Mohamedsedik, L. J. Li, L. Wang, O. Amat, L. N. Hu, and B. S. Xie, Phase effect and symmetry on pair production in spatially inhomogeneous frequency chirping electric fields, Eur. Phys. J. Plus **138**, 316 (2023).

[22] Z. L. Li, D. Lu, and B. S. Xie, Effects of electric field polarizations on pair production, Phys. Rev. D **92**, 085001 (2015).

[23] C. Kohlfürst, Phase-space analysis of the Schwinger effect in inhomogeneous electromagnetic fields, Eur. Phys. J. Plus **133**, 191 (2018).

[24] O. Olugh, Z. L. Li, and B. S. Xie, Dynamically assisted pair production for various polarizations, Phys. Lett. B **802**, 135259 (2020).

[25] Y. Ren, C. Luo, and I. Sitiwaldi, Dynamically assisted Schwinger mechanism in spatially separated electric fields, Phys. Rev. A **107**, 012210 (2023).

[26] I. A. Aleksandrov and C. Kohlfürst, Pair production in temporally and spatially oscillating fields, Phys. Rev. D **101**, 096009 (2020).

[27] C. Kohlfürst, Pair production in circularly polarized waves, arXiv:2212.03180.

[28] C. K. Dumlu and G. V. Dunne, The Stokes Phenomenon and Schwinger Vacuum Pair Production in Time-Dependent Laser Pulses, Phys. Rev. Lett. **104**, 250402 (2010).

[29] C. K. Dumlu and G. V. Dunne, Interference effects in Schwinger vacuum pair production for time-dependent laser pulses, Phys. Rev. D **83**, 065028 (2011).

[30] E. Akkermans and G. V. Dunne, Ramsey Fringes and Time-Domain Multiple-Slit Interference from Vacuum, Phys. Rev. Lett. **108**, 030401 (2012).

[31] R. Schutzhold, H. Gies, and G. Dunne, Dynamically Assisted Schwinger Mechanism, Phys. Rev. Lett. **101**, 130404 (2008).
[32] F. Hebenstreit, R. Alkofer, and H. Gies, Particle Self-Bunching in the Schwinger Effect in Spacetime-Dependent Electric Fields, Phys. Rev. Lett. **107**, 180403 (2011).
[33] F. Hebenstreit, Schwinger effect in inhomogeneous electric fields, Ph.D. thesis, University of Graz, arXiv:1106.5965.
[34] C. Kohlfürst, Electron-positron pair production in inhomogeneous electromagnetic fields, Ph.D. thesis, University of Graz, arXiv:1512.06082.
[35] O. Amat, L. N. Hu, A. Sawut, M. Mohamedsedik, M. A. Bake, and B. S. Xie, Schwinger pair production rate and time for some space-dependent fields via worldline instantons formalism, Eur. Phys. J. D **76**, 188 (2022).
[36] I. K. Affleck, O. Alvarez, and N. S. Manton, Pair production at strong coupling in weak external fields, Nucl. Phys. **B197**, 509 (1982).
[37] G. V. Dunne, Q. H. Wang, H. Gies, and C. Schubert, Worldline instantons. II. The fluctuation prefactor, Phys. Rev. D **73**, 065028 (2006).
[38] G. V. Dunne and Q. H. Wang, Multidimensional worldline instantons, Phys. Rev. D **74**, 065015 (2006).
[39] G. V. Dunne and C. Schubert, Pair creation in inhomogeneous fields from worldline instantons, AIP Conf. Proc. **857**, 240 (2006).
[40] G. V. Dunne, Worldline instantons, vacuum pair production and Gutzwiller's trace formula, J. Phys. A **41**, 164041 (2008).
[41] G. V. Dunne, New strong-field QED effects at ELI: Nonperturbative vacuum pair production, Eur. Phys. J. D **55**, 327340 (2009).
[42] C. K. Dumlu and G. V. Dunne, Complex worldline instantons and quantum interference in vacuum pair production, Phys. Rev. D **84**, 125023 (2011).
[43] B. S. Xie, M. Mohamedsedik, and S. Dulat, Electron-positron pair production in an elliptic polarized time varying field, Chin. Phys. Lett. **29**, 021102 (2012).
[44] A. Ilderton, G. Torgrimsson, and J. Wårdh, Pair production from residues of complex worldline instantons, Phys. Rev. D **92**, 025009 (2015).
[45] A. Ilderton, G. Torgrimsson, and J. Wårdh, Nonperturbative pair production in interpolating fields, Phys. Rev. D **92**, 065001 (2015).
[46] C. Schneider and R. Schützhold, Dynamically assisted Sauter-Schwinger effect in inhomogeneous electric fields, J. High Energy Phys. 02 (2016) 164.
[47] B. S. Xie, Z. L. Li, and S. Tang, Electron-positron pair production in ultrastrong laser fields, Matter Radiat. Extremes **2**, 225 (2017).
[48] C. Schneider, G. Torgrimsson, and R. Schützhold, Discrete worldline instantons, Phys. Rev. D **98**, 085009 (2018).
[49] K. Rajeev, Lorentzian worldline path integral approach to Schwinger effect, Phys. Rev. D **104**, 105014 (2021).
[50] G. Degli Esposti and G. Torgrimsson, Worldline instantons for nonlinear Breit-Wheeler pair production and Compton scattering, Phys. Rev. D **105**, 096036 (2022).
[51] G. Degli Esposti and G. Torgrimsson, Worldline instantons for the momentum spectrum of Schwinger pair production in spacetime dependent fields, Phys. Rev. D **107**, 056019 (2023).
[52] I. Bialynicki-Birula, P. Gornicki, and J. Rafelski, Phase space structure of the Dirac vacuum, Phys. Rev. D **44**, 1825 (1991).
[53] O. Olugh, Z. L. Li, B. S. Xie, and R. Alkofer, Pair production in differently polarized electric fields with frequency chirps, Phys. Rev. D **99**, 036003 (2019).
[54] Z. L. Li, C. Gong, and Y. J. Li, Study of pair production in inhomogeneous two-color electric fields using the computational quantum field theory, Phys. Rev. D **103**, 116018 (2021).
[55] C. Kohlfürst, F. Queisser, and R. Schützhold, Dynamically assisted tunneling in the impulse regime, Phys. Rev. Res. **3**, 033153 (2021).
[56] C. Kohlfürst, N. Ahmadiniaz, J. Oertel, and R. Schützhold, Sauter-Schwinger Effect for Colliding Laser Pulses, Phys. Rev. Lett. **129**, 241801 (2022).
[57] P. Krekora, Q. Su, and R. Grobe, Klein Paradox in Spatial and Temporal Resolution, Phys. Rev. Lett. **92**, 040406 (2004).
[58] P. Krekora, Q. Su, and R. Grobe, Interpretational difficulties in quantum field theory, Phys. Rev. A **73**, 022114 (2006).
[59] S. Tang, B. S. Xie, D. Lu, H. Y. Wang, L. B. Fu, and J. Liu, Electron-positron pair creation and correlation between momentum and energy level in a symmetric potential well, Phys. Rev. A **88**, 012106 (2013).
[60] L. Wang, B. Wu, and B. S. Xie, Electron-positron pair production in an oscillating Sauter potential, Phys. Rev. A **100**, 022127 (2019).
[61] L. Wang, L. J. Li, M. Mohamedsedik, R. An, J. J. Li, B. S. Xie, and F. S. Zhang, Enhancement of electron-positron pairs in combined potential wells with linear chirp frequency, Chin. Phys. B **32**, 010301 (2023).
[62] V. S. Popov, Imaginary-time method in quantum mechanics and field theory, Phys. At. Nucl. **68**, 686 (2005).
[63] Y. Kluger, E. Mottola, and J. M. Eisenberg, The quantum Vlasov equation and its Markov limit, Phys. Rev. D **58**, 125015 (1998).
[64] S. M. Schmidt, D. Blaschke, G. Ropke, S. A. Smolyansky, A. V. Prozorkevich, and V. D. Toneev, A quantum kinetic equation for particle production in the Schwinger mechanism, Int. J. Mod. Phys. E **07**, 709 (1998).
[65] Z. L. Li, D. Lu, and B. S. Xie, Multiple-slit interference effect in the time domain for boson pair production, Phys. Rev. D **89**, 067701 (2014).
[66] Z. L. Li, D. Lu, B. S. Xie, L. B. Fu, J. Liu, and B. F. Shen, Enhanced pair production in strong fields by multiple-slit interference effect with dynamically assisted Schwinger mechanism, Phys. Rev. D **89**, 093011 (2014).
[67] C. Gong, Z. L. Li, Y. J. Li, Q. Su, and R. Grobe, Resolving rapidly chirped external fields with Dirac vacuum, Phys. Rev. A **101**, 063405 (2020).
[68] V. S. Popov, Pair production in a variable external field (Quasiclassical approximation), Zh. Eksp. Teor. Fiz. **61**, 1334 (1971).
[69] S. P. Kim and D. N. Page, Improved approximations for fermion pair production in inhomogeneous electric fields, Phys. Rev. D **75**, 045013 (2007).

[70] E. Strobel and S. S. Xue, Semiclassical pair production rate for rotating electric fields, Phys. Rev. D **91**, 045016 (2015).
[71] J. Oertel and R. Schützhold, WKB approach to pair creation in spacetime-dependent fields: The case of a spacetime-dependent mass, Phys. Rev. D **99**, 125014 (2019).
[72] V. I. Ritus, Quantum effects of the interaction of elementary particles with an intense electromagnetic field, J. Russ. Laser Res. **6**, 497 (1985).
[73] A. I. Titov, B. Kämpfer, and H. Takabe, Nonlinear Breit-Wheeler process in short laser double pulses, Phys. Rev. D **98**, 036022 (2018).
[74] S. Tang, A. Ilderton, and B. King, One-photon pair-annihilation in pulsed plane-wave backgrounds, Phys. Rev. A **100**, 062119 (2019).
[75] A. Ilderton, Coherent quantum enhancement of pair production in the null domain, Phys. Rev. D **101**, 016006 (2020).
[76] B. King, Uniform locally constant field approximation for photon-seeded pair production, Phys. Rev. A **101**, 042508 (2020).
[77] D. Seipt and B. King, Spin- and polarization-dependent locally-constant-field-approximation rates for nonlinear Compton and Breit-Wheeler processes, Phys. Rev. A **102**, 052805 (2020).
[78] T. N. Wistisen, Numerical approach to the semiclassical method of pair production for arbitrary spins and photon polarization, Phys. Rev. D **101**, 076017 (2020).
[79] S. Lei, Z. Bu, W. Wang, B. Shen, and L. Ji, Generation of relativistic positrons carrying intrinsic orbital angular momentum, Phys. Rev. D **104**, 076025 (2021).
[80] T. Podszus and A. Di Piazza, First-order strong-field QED processes including the damping of particle states, Phys. Rev. D **104**, 016014 (2021).
[81] Z. Bu, L. Ji, S. Lei, H. Hu, X. Zhang, and B. Shen, Twisted Breit-Wheeler electron-positron pair creation via vortex gamma photons, Phys. Rev. Res. **3**, 043159 (2021).
[82] S. Tang, Fully polarized nonlinear Breit-Wheeler pair production in pulsed plane waves, Phys. Rev. D **105**, 056018 (2022).
[83] A. Golub, S. Villalba-Chávez, and C. Müller, Nonlinear Breit-Wheeler pair production in collisions of bremsstrahlung γ quanta and a tightly focused laser pulse, Phys. Rev. D **105**, 116016 (2022).
[84] A. J. MacLeod, P. Hadjisolomou, T. M. Jeong, and S. V. Bulanov, All-optical nonlinear Breit-Wheeler pair production with γ-flash photons, Phys. Rev. A **107**, 012215 (2023).
[85] N. B. Narozhnyi and A. I. Nikishov, Simplest processes in the pair-creating electric field, Yad. Fiz. **11**, 1072 (1970) [Sov. J. Nucl. Phys. **11**, 596 (1970)].
[86] E. Brezin and C. Itzykson, Pair production in vacuum by an alternating field, Phys. Rev. D **2**, 1191 (1970).
[87] F. Hebenstreit, R. Alkofer, and H. Gies, Schwinger pair production in space and time-dependent electric fields: Relating the Wigner formalism to quantum kinetic theory, Phys. Rev. D **82**, 105026 (2010).
[88] G. V. Dunne, *Heisenberg-Euler Effective Lagrangians: Basics and Extensions*, edited by M. Shifman *et al.*, From Fields to Strings Vol. 1 (World Scientific, Singapore, 2012), pp. 445–522.
[89] I. A. Aleksandrov, G. Plunien, and V. M. Shabaev, Locally-constant field approximation in studies of electron-positron pair production in strong external fields, Phys. Rev. D **99**, 016020 (2019).
[90] C. Kohlfürst, H. Gies, and R. Alkofer, Effective Mass Signatures in Multiphoton Pair Production, Phys. Rev. Lett. **112**, 050402 (2014).
[91] C. Kohlfürst, Spin-states in multiphoton pair production for circularly polarized light, Phys. Rev. D **99**, 096017 (2019).
[92] A. Blinne and E. Strobel, Comparison of semiclassical and Wigner function methods in pair production in rotating fields, Phys. Rev. D **93**, 025014 (2016).
[93] R. Landauer and T. Martin, Barrier interaction time in tunneling, Rev. Mod. Phys. **66**, 217 (1994).
[94] K. Y. Kravtcov, V. V. Dmitriev, S. A. Levenets, A. D. Panfyorov, S. A. Smolyansky *et al.*, The choice of the optimal approximation in the kinetic description of the vacuum creation of electron-positron plasma in strong laser fields, Proc. SPIE Int. Soc. Opt. Eng. **10717**, 1071702 (2018).
[95] I. A. Aleksandrov, A. D. Panferov, and S. A. Smolyansky, Radiation signal accompanying the Schwinger effect, Phys. Rev. A **103**, 053107 (2021).